

## Supplementary Materials for

### **Hydraulically amplified self-healing electrostatic actuators with muscle-like performance**

E. Acome, S. K. Mitchell, T. G. Morrissey, M. B. Emmett, C. Benjamin, M. King,  
M. Radakovitz, C. Keplinger\*

\*Corresponding author. Email: christoph.keplinger@colorado.edu

Published 5 January 2018, *Science* **359**, 61 (2018)  
DOI: 10.1126/science.aaq6139

#### **This PDF file includes:**

Materials and Methods  
Figs. S1 to S16  
References  
Captions for movies S1 to S8

#### **Other supplementary material for this manuscript includes the following:**

Movies S1 to S8

## **Materials and Methods**

### Materials

All hydraulically amplified self-healing electrostatic (HASEL) actuators consisted of three main components: an elastomeric shell, a flexible or stretchable electrode based on ionic conductors, and a liquid dielectric.

### Elastomeric shells

The elastomeric shells were made from either Ecoflex 00-30 (Smooth-on) or polydimethylsiloxane (PDMS) (Sylgard 184, Dow-Corning), which are both silicone elastomers. Ecoflex 00-30 was prepared by mixing a 1:1 ratio of parts A and B then degassing in a vacuum desiccator for at least 5 minutes. Uncured Ecoflex 00-30 was cast into a mold then cured in an oven at 70 °C for 10 minutes. PDMS was prepared by mixing a 10:1 ratio of base to cross-linker then degassing in a vacuum desiccator until all the air bubbles were removed. Uncured PDMS was cast into a mold then cured in an oven at 75 °C for 30 minutes. Different molds were used depending on the actuator size. Molds were machined from either aluminum or acrylic.

### Ionic conductors

Stretchable electrodes based on ionic conductors were synthesized from polyacrylamide (PAM) hydrogels containing lithium chloride (LiCl) (34).

PAM-LiCl hydrogels were composed of aqueous lithium chloride (LiCl; The Science Company, NC-4851) as the ionic conductor, acrylamide (AAm; Sigma, A8887) as the monomer, N,N-methylenebisacrylamide (MBAA; Sigma, 146072) as the crosslinker,

ammonium persulfate (AP; Sigma, 248614) as the photo-initiator, and N,N,N',N'-tetramethylethylenediamine (TEMED; Sigma, T9281) as the crosslinking accelerator.

PAM-LiCl hydrogels were synthesized by first dissolving LiCl (8 M) in deionized water and allowing the solution to cool to room temperature. AAm (2.2 M) was dissolved in the 8 M LiCl solution along with MBAA (0.06 wt% of AAm) and AP (0.17 wt% of AAm). The solution was mixed on a stir plate for 5 minutes then degassed for 10 minutes. To initiate polymerization, TEMED (0.05 wt% of AAm) was added to the solution immediately before casting the hydrogels. The hydrogels were cured under 365-nm UV light (3UV-38, UVP) for 1 h. Depending on the specific application of the electrodes, the hydrogel solution was cast in two different manners to create flexible or stretchable electrodes, as explained in the following two paragraphs.

### Flexible electrodes

The donut HASEL actuators used flexible electrodes of PAM-LiCl hydrogels (thickness of 200  $\mu\text{m}$ ) cast onto a 25.4  $\mu\text{m}$  thick Kapton film (Dupont, 5-50-KHN-1). The Kapton film acted as a protective backing which made the hydrogels easier to handle and restricted the electrode to being flexible, but not stretchable. Electrodes of desired shape and dimension were laser cut (Legend 36 EXT, Epilog) from the cast hydrogel sheets.

### Stretchable electrodes

The circular dielectric elastomer (DE) actuators and planar HASEL actuators used stretchable electrodes of PAM-LiCl hydrogels bonded directly to the surface of the elastomeric shell. To bond hydrogels to the elastomeric shell, the surface of the elastomer

was treated with benzophenone (B9300, Sigma Aldrich) (35). Before the benzophenone treatment, the surface of the elastomer was cleaned with methanol, then rinsed with deionized water and dried with compressed air. Then, the elastomer was masked with a laser-cut acrylic stencil to contain the benzophenone solution (10 wt% in ethanol) to the desired electrode area. A benzophenone solution (10 wt% in ethanol) was applied to the elastomer surface for two minutes then rinsed off three times with methanol. Once the surface was dried with compressed air, a 125  $\mu\text{m}$  thick polyethylene (PE) spacer cut out in the shape of the electrode was aligned with the treated area of the elastomer surface. The PAM-LiCl hydrogel solution was poured into the cutout of the spacer, covered with a glass slide, and cured under 365-nm UV light for 1h. The glass slide can be held in place using light-duty clamps. This process is shown in steps 1-3 of Figure S7.

### Liquid dielectric

The liquid dielectric used was commercially available Envirotemp FR3 (Cargill), which is formulated from vegetable oils and made for use in high-voltage transformers.

### Fabrication of donut HASEL actuators

Unless otherwise specified, the donut HASEL actuators used in this text were fabricated using the following procedure. PDMS was cast into 0.3 mm thick, 6 cm diameter circular sheets (Fig. S1, step 1) and cured in an oven at 75 °C for 30 minutes. An acrylic ring with a 6 cm outer diameter and 5 cm inner diameter was placed on top of each PDMS sheet such that the ring and sheet were concentric. Uncured PDMS was then applied on the area of PDMS sheet which overlapped with the acrylic ring (Fig. S1, step 2). Two PDMS

sheets were aligned concentrically and clamped between the acrylic rings, with the uncured PDMS between the sheets to act as a bonding agent (Fig. S1, step 2). A syringe with a needle was inserted between the clamped PDMS sheets, and air was used to inflate the shell to keep the middle from bonding together. The inflated shell was cured in an oven at 75 °C for 30 minutes (Fig. S1, step 3). Once cured, the clamps and acrylic rings were removed from the shell. An Ecoflex 00-30 patch was applied to a region of the PDMS shell to act as a fill point, which resealed after being punctured with a needle (Fig. S1, step 4). A syringe with a needle was inserted through the Ecoflex 00-30 patch, and then used to replace the air in the shell with 4 mL of liquid dielectric (EnviroTemp FR3) (Fig. S1, step 5).

After the PDMS shell was filled with liquid dielectric, circular flexible electrodes (PAM-LiCl hydrogel on Kapton film) were placed on either side of the shell, with the Kapton film facing outward (Fig. S1, step 6) and with the leads oriented 180° from each other. The PDMS shell and electrodes were aligned concentric to each other and glued in place with cyanoacrylate glue (406, Loctite).

### Hydraulic scaling of donut HASEL actuators

Two donut HASEL actuators were fabricated, one having an electrode diameter of 2.5 cm (Fig. 1D), while the other had an electrode diameter of 1.5 cm (Fig. 1E). The strain of actuation was measured for ten different amplitudes of the voltage signal (0 to 20 kV, in increments of 2 kV) and under different loads. The voltage signals applied to the actuator used a 0.5 Hz square waveform with reversing polarity at a duty cycle of 50%. This

waveform (Fig. S2) was selected to counteract the accumulation of static charge on the PDMS shell between cycles.

At a fixed amplitude of voltage, load on the actuators was varied from no load to the blocking load. A cantilever beam constructed out of Lego© bricks was used to stabilize the loads that were applied to the actuators. The loads applied to the actuator in Fig. 1D and 1E ranged from 50-250 g and 50-400 g, respectively, and were applied in 50 g increments.

For each load and voltage signal combination, a video of the response of actuation was recorded using a DSLR camera (EOS 6D, Canon), and the strain of actuation was measured using ImageJ (version 1.49v).

#### Measurement of electromechanical efficiency

The electromechanical efficiency of a HASEL actuator is based on the mechanical (output) energy and the electrical (input) energy expended during a complete cycle of actuation. To determine electromechanical efficiency of a donut HASEL actuator with electrode diameter of 2.5 cm (Fig. 1C), we performed the cycle illustrated in Fig. S4A. The four steps of the cycle were as follows:

**1 → 2:** The actuator started with a constant load of 100 g and at zero voltage. A linear voltage ramp was applied to charge the actuator with electrical energy. As voltage increased, the electrodes pulled together and caused the actuator to increase in thickness. This deformation enabled the donut HASEL to perform mechanical work by lifting the 100 g load.

**2 → 3:** At the maximum values for voltage and displacement, the load was removed from the actuator.

**3 → 4:** The actuator was discharged by linearly decreasing voltage. The donut HASEL actuator returned to the initial thickness at zero voltage. Since the load had been removed, no mechanical work was performed during this step.

**4 → 1:** The load was placed onto the actuator with voltage off. Neither electrical nor mechanical work was performed in this step.

We used the experimental setup seen in Fig. S4B to measure the electrical energy consumed and the mechanical work performed by the actuator during the cycle. A custom LabVIEW program (version 15.0.1f2, 64-bit) and a data acquisition board (DAQ) (Model USB6212, National Instruments) were used to provide a control signal to the high-voltage (HV) amplifier (Model 50/12, Trek). HASEL actuators are electrically equivalent to a variable capacitor,  $C$ , with a resistor in series,  $R_{\text{electrode}}$ , to represent resistance of the electrodes. Leakage current through the HASEL actuator is represented by a parallel resistor,  $R_{\text{leakage}}$ . Some electrical energy will be lost to electrode resistance and leakage current. The efficiency of HASEL actuators could be increased by reducing the amount of leakage current during actuation.

Electrical energy was determined by controlling the voltage,  $V(t)$ , applied to the actuator and measuring the current,  $I(t)$ , flowing in and out of the actuator. Voltage applied to the actuator,  $V(t)$ , was prescribed by the custom LabVIEW program and applied through the HV amplifier. Current,  $I(t)$ , was calculated using Ohm's law with measurement of voltage,  $V_m(t)$ , across a precision resistor,  $R_m = 2 \text{ k}\Omega$ . The precision resistor was placed on the ground side of the circuit and connected in parallel to a transient-voltage-suppression diode (Model 1.5KE56CA-TP, Micro Commercial Components) to protect the DAQ equipment in case dielectric breakdown occurred. Charge,  $Q(t)$ , was calculated by taking

the cumulative integral of current,  $I(t)$ , over time,  $t$ . Finally, electrical energy was calculated as the area enclosed by the path of the cycle within the voltage-charge work-conjugate plane (Fig. S4E).

Mechanical energy was determined by measuring the displacement of the load as a function of time. A high-speed camera (Model Phantom v710, Vision Research) was used to record video of the actuator from state 1 to 2 of the cycle described in Fig. S4A. Video analysis software (Tracker) was used to determine vertical displacement of the load,  $y(t)$ . Tracker was also used to determine the force accelerating the load during actuation. Mechanical energy was calculated as the area enclosed by the path of the cycle within the force-displacement work-conjugate plane (Fig. S4H).

The applied voltage signal,  $V(t)$ , was a symmetric triangle with 1.5 s total period (0.75 s charging and 0.75 s discharging) with an amplitude of 21 kV (Fig. S4C). The electrodes of the actuator were covered with a thin layer of Ecoflex 00-30 to reduce the loss of charges to the surroundings. The time variation of parameters for electrical energy (Fig. S4C-E) are plotted beside their corresponding mechanical parameters (Fig. S4F-H). A pull-in transition occurs around 0.5 s, which is indicated by a sudden change in current and charge (Fig. S4D) as well as a sudden change in displacement (Fig. S4G). The area enclosed by the path of the actuator in the voltage-charge work-conjugate plane (Fig. S3E) represents the electrical energy,  $W_{\text{el}}$ , which was 2.88 mJ. Likewise, the area enclosed by the path of the actuator in the force-displacement work-conjugate plane (Fig. S4H) represents the mechanical energy of the cycle,  $W_{\text{mech}}$ , which was 0.59 mJ. The corresponding efficiency,  $W_{\text{mech}}/W_{\text{el}}$ , was 21%.

### Demonstration of self-healing capabilities of donut HASEL actuators

A donut HASEL actuator was fabricated as described in the *Fabrication of donut HASEL actuators* section, with the exception that the elastomeric shell was made of 0.5 mm thick Ecoflex 00-30 circular sheets with a diameter of 8 cm. These larger sheets resulted in a 1.5 cm wide skirt surrounding the 5-cm diameter shell. This skirt provided additional insulation against dielectric breakdown through air. When initially attempting this experiment with PDMS as the elastomeric shell, breakdown through air would occur before breakdown through the solid and liquid dielectrics; and thus, Ecoflex 00-30 was chosen as the elastomeric shell material because it yielded a lower breakdown strength as compared to PDMS. The electrode diameter was 1.5 cm. A linear voltage ramp was applied to the actuator at a rate of 1 kV/s until dielectric breakdown occurred. The high voltage amplifier (Model 50/12, Trek) was set to trip once the current hit a limit of 1.2 mA, which prevented dielectric breakdown from burning a large hole into the elastomeric shell. Additionally, the LabVIEW program used to generate the voltage ramp shut off the low voltage signal to the high voltage amplifier within 10 ms of the current reaching the limit level (1.2 mA). After each dielectric breakdown, a 10-s wait period was enacted before another voltage ramp of 1 kV/s was applied. This process was repeated 50 times.

### Comparison of dielectric breakdown through liquid and solid dielectrics

A chamber made from acrylic (35 x 30 x 10 mm) was filled with either solid or liquid dielectric to demonstrate the dielectric breakdown characteristics of each material (Fig. S5A). Commercially available nickel-plated T-pins (1.11 mm maximum diameter, 38.1 mm length) were used as the oppositely charged electrodes. The T-pins were inserted into

each end of the chamber with a tip separation distance of 0.5 mm. The chamber was filled with either solid dielectric material (PDMS, Sylgard 184, Dow Corning) or liquid dielectric material (Envirotemp FR3, Cargill). The PDMS was degassed in a vacuum desiccator for at least 60 minutes, then cured in an oven at 70 °C for 60 minutes. The liquid dielectric was degassed for at least 60 minutes prior to testing to ensure that all air bubbles were removed.

One T-pin was connected to the electrical ground while the other was connected to the high voltage amplifier (Model 50/12, Trek). The high voltage signal was linearly increased at a rate of 0.5 kV/s until dielectric breakdown occurred. Video of the breakdown event was recorded at 60 frames per second with a DSLR camera and images were selected at difference stages of dielectric breakdown in both solid (Fig. S5B) and liquid (Fig. S5C) dielectrics.

### Construction of donut HASEL stacks

Donut HASEL actuators were stacked such that the adjacent electrodes of neighboring actuators were connected to the same lead from the power supply, as seen in Fig. 2A. This design ensured that adjacent electrodes were at the same potential to avoid a short circuit between neighboring actuators. All donut HASEL actuator stacks were actuated using the waveform described in the *Hydraulic scaling of donut HASEL actuators* section and shown in Fig. S2.

### Fabrication of a soft gripper based on donut HASEL actuators

Donut HASEL actuators were fabricated as described in the *Fabrication of donut HASEL actuators* section with the exception that the PDMS sheets had a diameter of 8 cm.

The 8-cm diameter PDMS sheets resulted in a 1.5 cm wide skirt surrounding a 5 cm diameter shell. Ten donut HASEL actuators were constructed in this way and the skirt was cut away from half of the circumference of each actuator. Stacks of five donut HASEL actuators were constructed by bonding the skirt of each actuator together using uncured PDMS. A fabricated stack of five donut HASEL actuators is shown in Fig. S6A and S6B. The added constraint from bonding the donut HASEL actuators together on one side produced a tilting motion upon application of voltage. The stacks were mounted to opposing sides of an acrylic frame using double sided tape with the ground electrodes facing inwards (Fig. S6C, Fig. 2C and D).

#### Comparison of DE actuators with HASEL actuators

Circular DE and circular HASEL actuators were fabricated to have the same overall dielectric thickness (Fig. 3A). The total dielectric thickness  $t$  (1.5 mm) was chosen for ease of handling and fabrication. Acrylic molds were machined to various thicknesses for casting the elastomer shells (Ecoflex 00-30) in the same manner described in the *Elastomeric shells* section.

The elastomer for the circular DE actuator was made from a single piece of Ecoflex 00-30 (5 cm in diameter and 1.5 mm thick). The stretchable electrodes were cured and bonded (described below) to one side of the elastomeric shell at a time. For durability and electrical insulation, an encapsulating layer of Ecoflex 00-30 was spin-coated over the stretchable electrodes.

The elastomeric shell for the circular HASEL actuator was made from two pieces of Ecoflex 00-30. One piece was a 0.5 mm thick disk measuring 5 cm in diameter. The other

piece was a 1 mm thick disk, also 5 cm in diameter, and included a debossed region in the center of the disk that was 0.5 mm deep and 2.25 cm in diameter. The debossed region was filled with liquid dielectric after the two halves are bonded together. A stretchable electrode was cured and bonded to each piece of the elastomeric shell (described below). For durability and electrical insulation, an encapsulating layer of Ecoflex 00-30 was spin-coated over the stretchable electrodes. Uncured Ecoflex 00-30 was then used to bond the two halves of the elastomer shell together. A needle with a syringe was used to fill the middle volume with air to prevent the shell from bonding together. The assembled elastomer shell was cured in an oven at 70 °C for 10 minutes. A syringe with a needle was then used to remove the air and fill the empty volume with 0.2 mL of liquid dielectric (Envirotemp FR3).

For both circular DE and HASEL actuators, stretchable electrodes with a diameter of 2 cm were bonded and cured to the surface of the elastomer in the same manner described in the *Stretchable electrodes* section with the exception of adding yellow food dye (McCormick) to the hydrogel to increase optical contrast, making it possible to automatically record strain with a custom MATLAB program. We found that including dye in the PAM-LiCl precursor solution affected crosslinking of the hydrogel. To circumvent this issue, we modified the process described in the *Stretchable electrodes* section by replacing the 8 M LiCl solution with deionized water to make PAM hydrogels. After curing and bonding the PAM hydrogels to the elastomer surface, the hydrogel was dried and then swollen with a solution of yellow dye and 8 M LiCl.

Once fully fabricated, the actuators were biaxially prestretched 1.5 times and clamped between two acrylic rings. Toothless alligator clips were used to connect one electrode to

ground and the other electrode was connected to a high voltage amplifier (Model 50/12, Trek). DC voltage was applied to the actuators and increased in steps of 0.5 kV until electric breakdown occurred. There was a 15 s interval between each step to account for viscoelastic effects. Video of each actuator was recorded and used to measure area strain as a function of applied voltage.

A custom video processing program in MATLAB (Version 9.0, R2016a) was used to measure the area of the electrodes as voltage increased (code included in *Algorithm for image processing*). Video was imported to the MATLAB program and each frame was analyzed individually. Every frame was isolated into a single RGB layer and a matrix of the intensity values for each pixel was built. A binary mask was created by setting each value in the matrix to either 0 (black) or 255 (white). The threshold for the binary mask could be varied depending on the contrast of the electrodes with the rest of the frame. Next, a function scanned through each column of the binary mask matrix and recorded the number of cells with a 0 value. It was assumed that the electrode is a perfect circle and the column with the most 0 valued cells was the diameter of the circular electrodes. The electrode area for that frame was then calculated in pixels squared and area strain was plotted as a function of time (Fig. S7A) and as a function of voltage (Fig. 3A and Fig. S7B). The accuracy of this program was confirmed by comparing values from the video processing program to those measured manually with ImageJ (Fig. S7B).

#### Fabrication of planar HASEL actuators

Planar HASEL actuators (Fig. S8) consisted of two identical elastomer (Ecoflex 00-30) shell pieces (6 cm wide x 9 cm long x 0.8 mm thick), which were formed by casting

the uncured elastomer into machined rectangular acrylic molds. Stretchable electrodes were patterned onto each shell piece as described in the *Stretchable electrodes* section, then encapsulated with Ecoflex 00-30 via spin-coating and cured in an oven at 70 °C for 10 minutes.

Two elastomer shell pieces patterned with hydrogels were bonded together using uncured Ecoflex 00-30. The two shell pieces were clamped between two laser-cut acrylic pieces with the electrodes facing outwards, and a syringe with a needle was used to create an air-filled pouch between the electrodes. After curing in an oven at 70 °C for 10 minutes, a syringe with a needle was used to replace the air within the shell with 1.2 mL of liquid dielectric (Envirotemp FR-3). An overall view of the components and assembly of a planar HASEL actuator are shown in Fig. S8. Individual steps for fabricating the planar HASEL actuators are illustrated in Fig. S9.

We refer to a single region of liquid dielectric as a HASEL unit for planar actuators. The maximum height of each unit was limited to 1.5 cm to prevent liquid dielectric from collecting at the bottom of the unit. The width of the single units can also be small to allow for operation in multiple orientations and the method for patterning hydrogels onto the elastomer surface makes it possible to fabricate electrodes of varying size and geometry (Fig. S10).

### Linear actuation with planar HASEL actuators

Planar HASEL actuators were used for linear actuation by applying a fixed prestretch in one direction (Fig. S11). This configuration has been used for DE actuators and is often referred to as ‘pure-shear’ because the elastomer is constrained like a sample for pure-shear

tests (29). Two ends of the planar HASEL actuator were stretched and clamped between two rectangular pieces of acrylic which were held together with plastic screws. One of the clamped ends was fixed while the other was attached to a hanging load, which resulted in a certain amount of prestretch in the direction of the load. When voltage was applied, the actuator expanded preferentially in the direction of the load.

Linear planar HASEL actuators were operated in quasi-static and dynamic modes. For quasi-static actuation, DC voltage was applied in increasing steps of 0.5 kV with 10 s between each step (Fig. 3C). For dynamic actuation, voltage was applied as a sine wave with minimum voltage of 0 kV and maximum voltage set manually. Actuation frequency was set near the resonant frequency to achieve 107% actuation strain for a single-unit (Fig. S11A) and 124% for a two-unit actuator (Fig. S11B). A single unit actuator, operated near resonance, lifted a 1.5 kg load (which corresponds to 0.3 MPa) over a linear actuation strain of 16% (Fig. S13). The resonance frequency was determined by manually changing frequency while observing the actuation strain.

#### Measurement of specific power and work of HASEL actuators

Gravimetric power and work were determined for a planar HASEL actuator lifting a mass,  $m$  (Fig. S12A). The power output,  $P(t)$ , of the linear planar HASEL actuator is equal to the time-derivative of the sum of potential ( $PE$ ) and kinetic energy ( $KE$ ) of the mass,  $m$ :

$$P(t) = \frac{d(KE)}{dt} + \frac{d(PE)}{dt} = \frac{d(\frac{1}{2}mv(t)^2)}{dt} + \frac{d(mgy(t))}{dt} = mv(t)[a(t) + g] \quad (S1)$$

where  $y(t)$  is vertical displacement,  $v(t)$  is velocity of the mass,  $a(t)$  is acceleration of the mass, and  $g$  is acceleration due to gravity. A high-speed camera (Model Phantom v710, Vision Research) was used to record actuation. Video analysis software (Tracker) was then

used to determine position, velocity, and acceleration of the mass (Fig. S12B). Gravimetric work performed by the actuator was calculated by integrating power with respect to time.

We measured gravimetric power and work for a two-unit and single-unit planar HASEL actuator. The two-unit actuator lifted a 700 g load at a frequency of 2.4 Hz and maximum voltage of 14.5 kV (Fig. S12B). Peak and average specific output power during contraction was 614 W/kg and 337 W/kg, respectively (Fig. S12C). Specific work during contraction was 70 J/kg. The single-unit actuator lifted a 1 kg load at a frequency of 3.8 Hz and maximum voltage of 9 kV. Peak and average specific output power during contraction was 586 W/kg and 358 W/kg, respectively (Fig. S12D). Specific work during contraction was 47 J/kg. The single-unit actuator provided 586 W/kg peak power during contraction for 158,061 cycles before failure from mechanical rupture.

### Self-healing with planar HASEL actuators

Self-healing tests were performed on a six-unit planar HASEL actuator by applying a linear voltage ramp at a rate of 0.5 kV/s until dielectric breakdown occurred. The device was left to rest for 1 minute after each dielectric breakdown before beginning another voltage ramp. This process was repeated for 50 self-healing cycles (Fig. S11). Initial breakdown voltage occurred at 11.4 kV which immediately produced a gas bubble and created a spot with low breakdown strength. Subsequent dielectric breakdown events occurred at this location because of the lower breakdown strength of the gas bubble. Once the gas was removed with a syringe with a needle, breakdown voltage returned to the same level as the initial dielectric breakdown event. Even without removing gas bubbles,

dielectric breakdown can occur in different locations of the same unit or in a completely different HASEL unit (Fig. S14).

### Self-sensing HASEL actuators

HASEL actuators can simultaneously function as actuators and sensors by driving actuation with a high-amplitude “actuation voltage signal”, while applying a superimposed high-frequency, low-amplitude AC “sensing voltage signal”. The actuation signal is responsible for providing the driving force for physical movement while the sensing signal is too low of an amplitude to influence the actuation.

HASEL actuators are hyper-elastic capacitors with capacitance calculated as:

$$C = \epsilon_0 \epsilon_R \frac{A}{d} \quad (\text{S2})$$

where  $\epsilon_0$  is vacuum permittivity,  $\epsilon_R$  is the relative permittivity of the material,  $A$  is the area of the electrodes, and  $d$  is the dielectric thickness between the electrodes. When the structure of a HASEL actuator is deformed by an external force or by an applied actuation voltage, the electrode area and/or dielectric thickness change, which results in a change in capacitance.

The electrical behavior of a HASEL actuator can be modeled as an RC circuit. Thus, the transient capacitance of an actuator can be determined by analyzing the impedance and phase shift between an applied AC voltage signal and current signal (13). The magnitude of the impedance,  $Z$ , is calculated as

$$|Z| = \frac{V_0}{I_0} \quad (\text{S3})$$

where  $V_0$  is the voltage and  $I_0$  is the current. The phase shift ( $\phi$ ) between current and voltage can be measured by comparing the voltage and current signals. Capacitive impedance,  $X_C$ , is calculated as

$$X_C = |Z|\sin(\phi) \quad (\text{S5})$$

Finally, the capacitance ( $C$ ) of the circuit can be calculated by using the capacitive impedance ( $X_C$ ) and the frequency,  $f$ , of the applied voltage signal:

$$C = \frac{1}{2\pi f X_C} \quad (\text{S5})$$

A custom LabVIEW program and a DAQ (Model USB-6212, National Instruments) were used to output combined actuation and sensing signals and receive signals from the high voltage amplifier (Model 50/12, Trek) (Fig. S15). The main virtual instrument (VI) of the LabVIEW program combined the sensing and actuation signals, then sent the superimposed signal to the DAQ. From the DAQ, the signal was sent as an analog output to the high voltage amplifier which had a constant gain of 5 kV/V. The high voltage output signal was applied to the HASEL actuator. Feedback from the current and voltage monitors of the HV amplifier were sent to the analog inputs of the DAQ which read the input signal at a rate of 20 kHz. The LabVIEW program used equations S3-5 to calculate capacitance from the voltage and current signals. Capacitance measurements were continuously calculated and recorded as a function of time.

### Algorithm for image processing

The following script was written for MATLAB (Version 9.0, R2016a) and was used to automatically measure area strain of circular HASEL and DE actuators (Fig. 3A and Fig. S7). It is written as a single function ‘AreaStrainProgram’ which contains five different

sub-functions. The script is commented throughout for clarity. An example filename of ‘HASEL.mp4’ is used below.

```
% Introductory Notes

% This program is written to analyze video with dimensions of 1280x720
% recorded at a frame rate of 60 frames/second. To change diameter
% measurement window for your specific video dimensions, modify range
% of indices in the for loop within circleDiameter function. To
% change frame rate, modify the 'time' variable within the GraphAreas
% function. If there is significant noise in the data, you should try
% several threshold values. If that does not help, try measuring every
% nth frame instead of every frame. Always verify the measurements of
% this algorithm by manually measuring some of the frames.

%%%%%%%%%%%%%%%
% User inputs

% There are two required user inputs,
% videoLocation - the filepath for the video to be analyzed

% Command Window prompts - The command window will ask for input
% after initial analysis for proper RGB channel and thresholding.

%%%%%%%%%%%%%%%
% end of notes

function [] = AreaStrainProgram ()
% AreaStrainProgram will calculate the area strain of the electrodes
% based on video of actuation

% Call RGBlayer function to determine best channel to use and
% threshold value

%%%%%%%%%%%%%%%
% USER INPUT
% please note the file path to video. Video format must be .mp4.
videoLocation='HASEL.mp4';

%%%%%%%%%%%%%%%
RGBlayer(videoLocation);

% Prompt user to input which channel has the highest contrast
prompt = 'What channel should be used? Input 1 for Red, 2 for Green,
or 3 for Blue: ';
channel = input(prompt);

% Prompt user to input threshold limit for binary mask - ideally in
% between maximum and minimum values for the channel
prompt1 = 'What is the threshold value for the binary mask? Pick value
between maximum and minimum values: ';
threshold = input(prompt1);
```

```

close all

% Call VideoProcess function to analyze video and create graph of
% strain vs time
VideoProcess(videoLocation,channel, threshold);
end

function [ ] = RGBlayer( filename )
% RBGlayer will plot pixel values for center of electrode to choose
% correct layer to analyze
% This function will look at values of RGB channels at the center of
% actuator
% Inputs:      filename: Enter as string e.g. 'HASEL.mp4'
% Outputs:     none

v = VideoReader(filename); % Read Video
img = read(v,1); % Load first frame into matrix
imgR = img(:,:,1); % Store red channel
imgG = img(:,:,2); % Store green channel
imgB = img(:,:,3); % Store blue channel
vecR = imgR(:,640); % Store red channel middle column
vecG = imgG(:,640); % Store green channel middle column
vecB = imgB(:,640); % Store blue channel middle column

% Plot Red Channel
subplot(1,3,1);
plot(vecR);
title('Red Channel');
ylim([0 170]);
% Plot Green Channel
subplot(1,3,2);
plot(vecG);
title('Green Channel');
ylim([0 170]);
% Plot Blue Channel
subplot(1,3,3);
plot(vecB);
title('Blue Channel');
ylim([0 170]);
end

function [ ] = VideoProcess(video, prompt,threshold)
% This function will look at every frame and calculate the area of the
% actuator in pixels squared
% Inputs:  video: Enter as string eg. 'HASEL.mp4'
v = VideoReader(video); % Read video

% Calculate total number of frames in the video
if true
    vidObj = VideoReader(video);
    read(vidObj, Inf);
    numframes = vidObj.NumberOfFrames;
end
numframes = floor(numframes);
storedAreas = zeros(numframes,1); % Pre-allocate "storedAreas" vector

for i = 1:numframes % Total number of frames in the video

```

```



```

```

diameter = max(black);
% Find max value of black in column, this is the diameter
end

function [ ] = GraphAreas(input)
% This function will create a graph of the area %
origdia = input(1); % Store initial area in variable
n = length(input);
for i = 1:n
    strain(i) = 100*(input(i)^2 - origdia^2)/origdia^2;
    % Calculate area strain for each point
end
frame = (1:n); % Generate frame vector
time = frame/60;
% Created time vector based on frame rate of 60 frames/s
plot(time,strain);
title('Graph of Area Strain v. Time');
xlabel('Time (s)');
ylabel('Strain (%)');

```

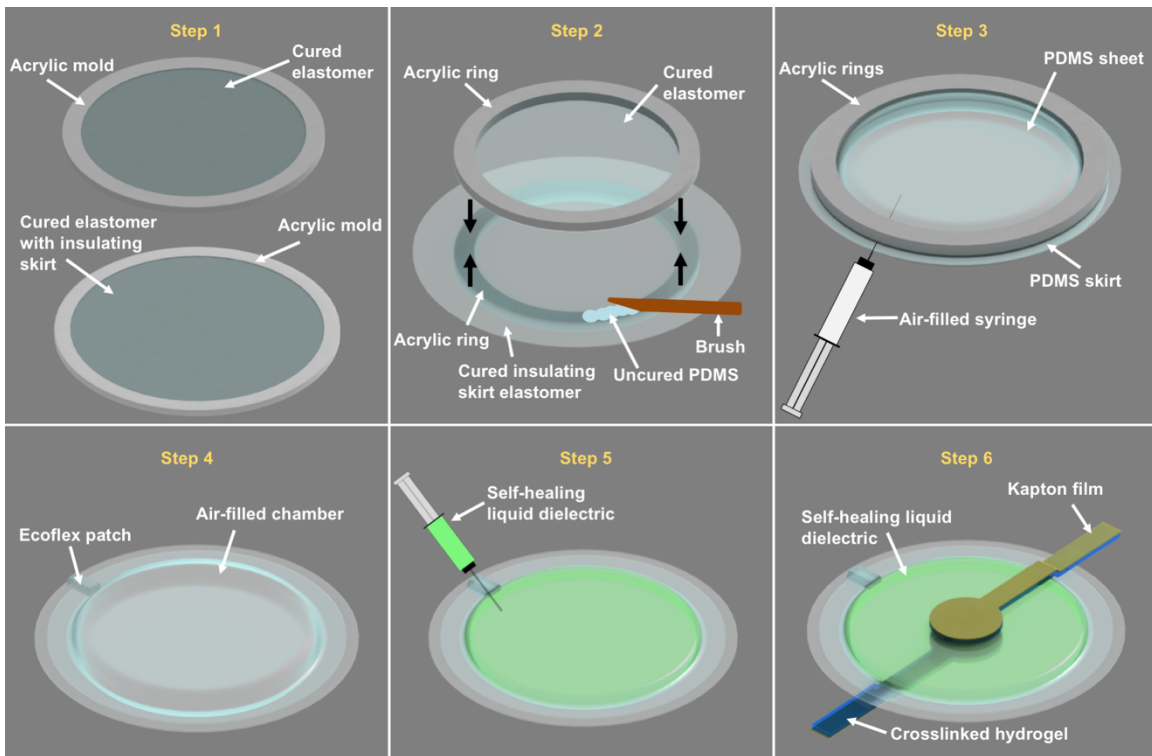


**Fig. S1. Fabrication steps for a donut HASEL actuator:** **Step 1** – Cast 0.3 mm thick PDMS sheets using acrylic molds. One sheet has a diameter of 6 cm and the other sheet has a diameter of 8 cm. The larger sheet acts as an insulating skirt to prevent dielectric breakdown through air. **Step 2** – Each sheet is aligned concentrically with an acrylic ring. Uncured PDMS is applied to the area which overlaps with the acrylic rings and the two halves are clamped together. **Step 3** – A needle and syringe is inserted between the two halves to inflate the shell. The clamped sheets are cured together in an oven at 75 °C for 30 minutes. **Step 4** – Remove the acrylic rings and apply an Ecoflex patch which acts as a fill port. **Step 5** – A syringe with a needle is inserted through the Ecoflex 00-30 patch then used to replace the air within the chamber with 4 mL of liquid dielectric. **Step 6** – Circular flexible electrodes (PAM-LiCl hydrogel on Kapton film) are placed on either side of the shell, with the Kapton film facing outward.

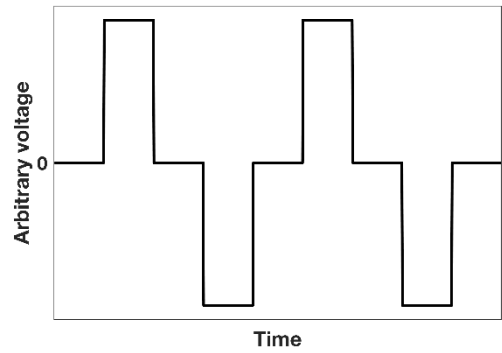


**Fig. S2. Voltage waveform used for actuation of donut HASEL actuators.** Voltage was applied as a square wave that switched polarity each actuation cycle.

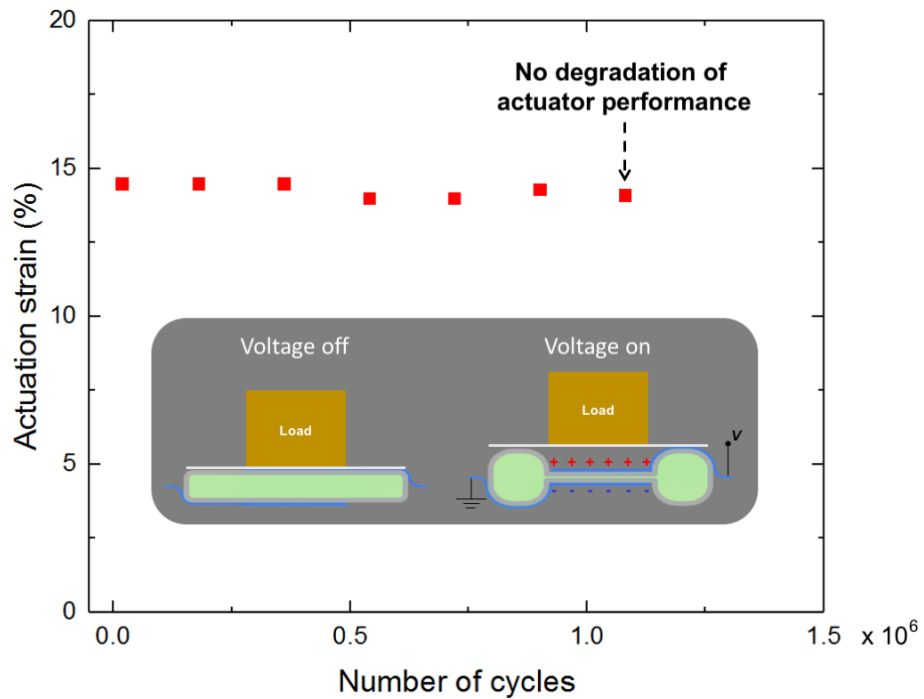


**Fig. S3. Cycle life of a donut HASEL actuator.** A donut HASEL actuator (Fig. 1E) was actuated with 18 kV at 5 Hz using the reversing polarity waveform seen in Fig. S2. Under an applied load of 150 g, the actuation strain of the device does not noticeably diminish over the course of 1.08 million cycles. The lifetime test was stopped due to time constraints and not due to failure of the actuator.

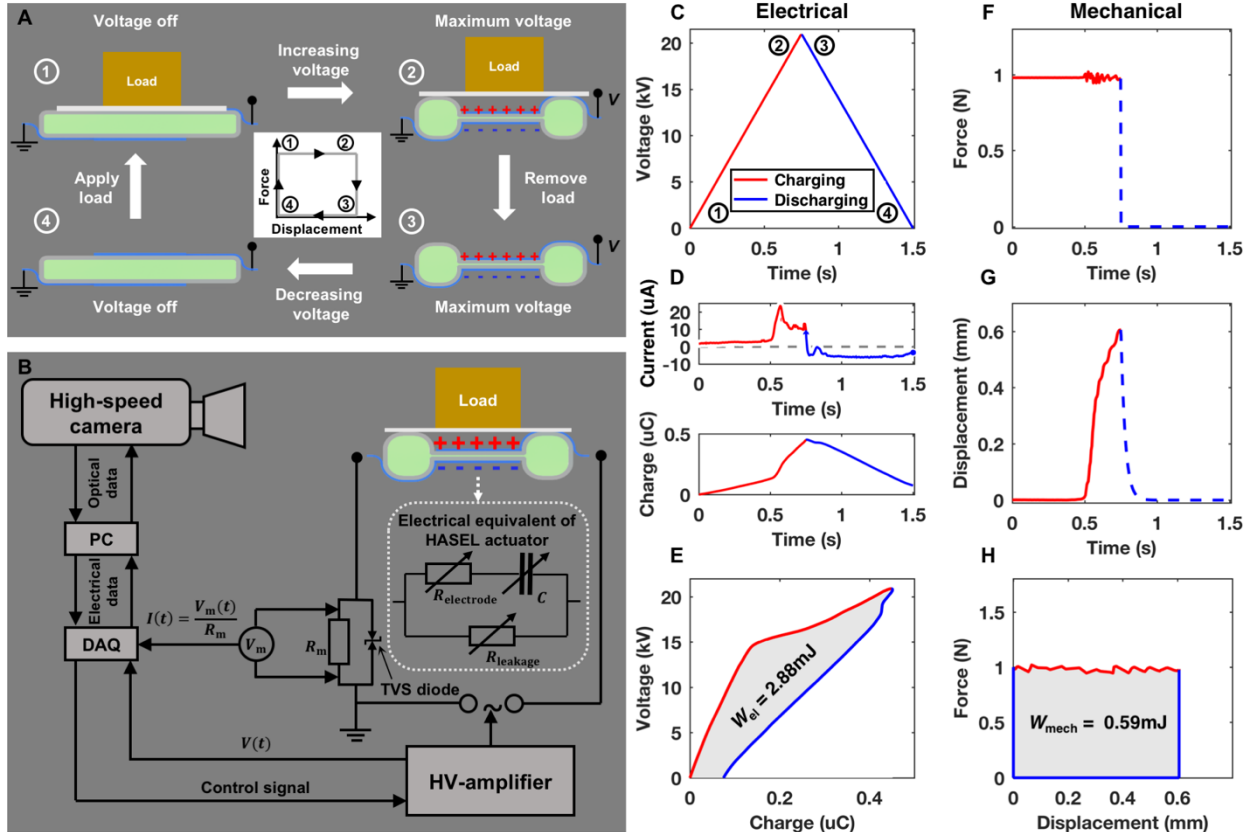


**Fig. S4. Electromechanical efficiency of a HASEL actuator.** (A) The actuation cycle used for measuring electromechanical efficiency of donut HASEL actuators. (B) The experimental setup for measuring efficiency: a high-speed camera was used to record displacement,  $y(t)$ . A DAQ sent a control signal to the HV-amplifier and recorded voltage,  $V(t)$ , and current  $I(t)$ . Electrical energy was calculated using voltage and current measurements. (C-E) Electrical measurements for actuation cycle of a donut-HASEL actuator lifting a 100 g load. (C) Voltage was applied as a symmetric triangular pattern with maximum voltage of 21 kV and period of 1.5 s. (D) A sudden increase in current and a change in the slope of charge indicates pull-in transition of the donut HASEL actuator. (E) Total electrical energy consumed was 2.88 mJ. (F-H) Time histories of mechanical variables during actuation were recorded for the same cycle. Total mechanical work or energy output was 0.59 mJ. Electromechanical efficiency for the cycle was 21%.

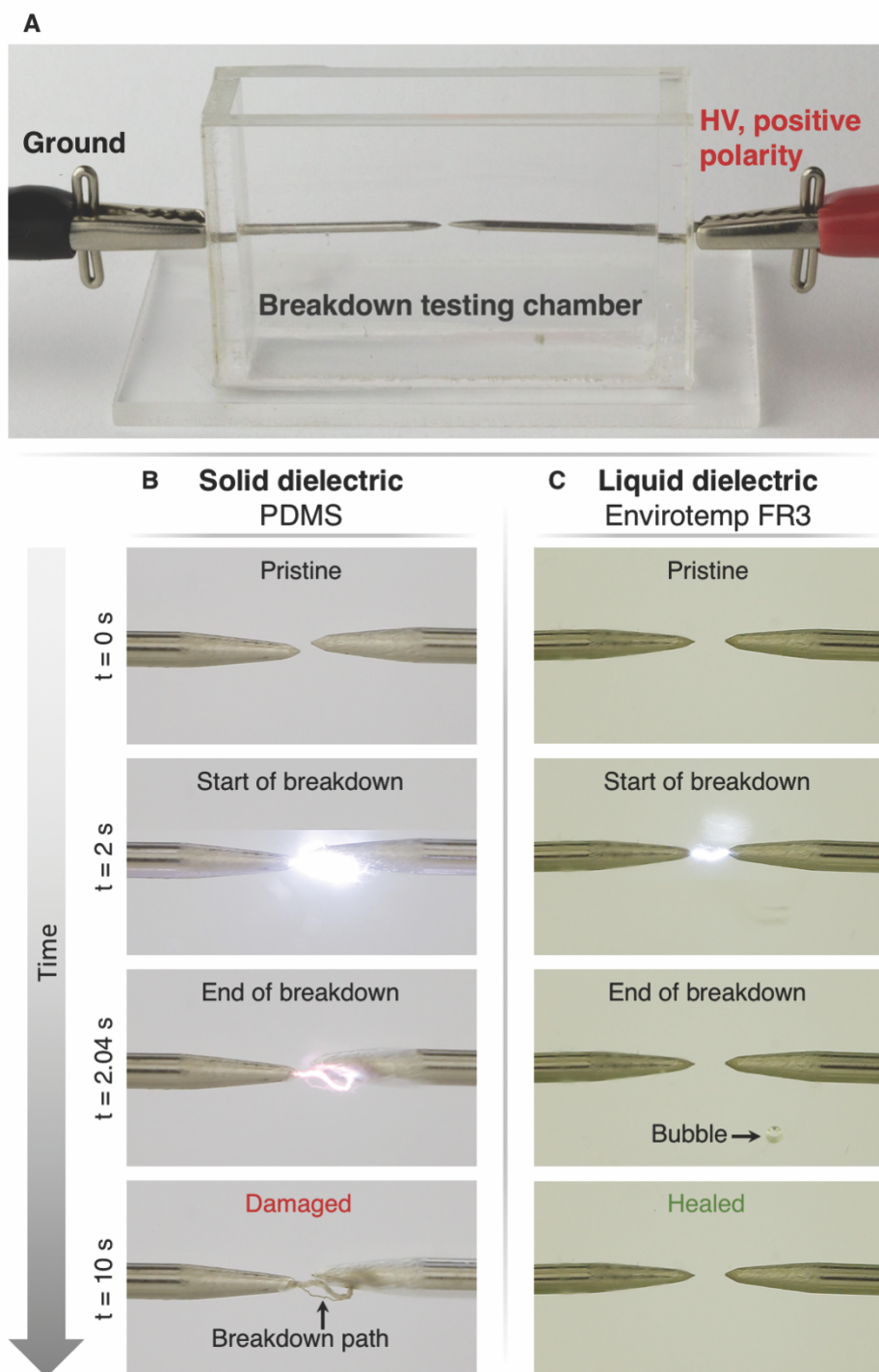


**Fig. S5. Comparison of dielectric breakdown in liquid and solid dielectric materials.**

(A) Breakdown testing chamber composed of acrylic box, T-pins, and electrical connections. (B) Sequence of dielectric breakdown through solid dielectric (PDMS): the

pristine dielectric material is shown at 0 s; breakdown started 2 s later at an applied voltage of 34.3 kV; electrical discharge through the material continued 0.04 s after breakdown was initiated; after dielectric breakdown, there was a permanent path left in the solid dielectric.

(C) Sequence of dielectric breakdown through liquid dielectric (Envirotemp FR3): the pristine dielectric material is shown at 0s; breakdown started 2 s later at an applied voltage of 14.7 kV and created only a small bubble; the bubble dissipated and the liquid dielectric was restored to an insulating state.

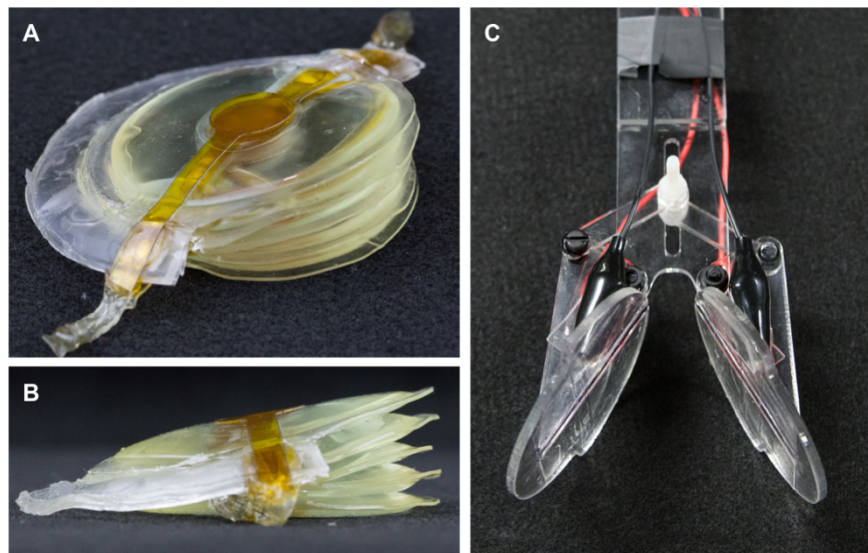


**Fig. S6. Soft gripper made from stacks of donut HASEL actuators.** (A) Isometric view and (B) side view of the donut HASEL stacks used for the soft gripper. (C) Side view of the acrylic component of the gripper used to hold the stacks in the proper orientation.

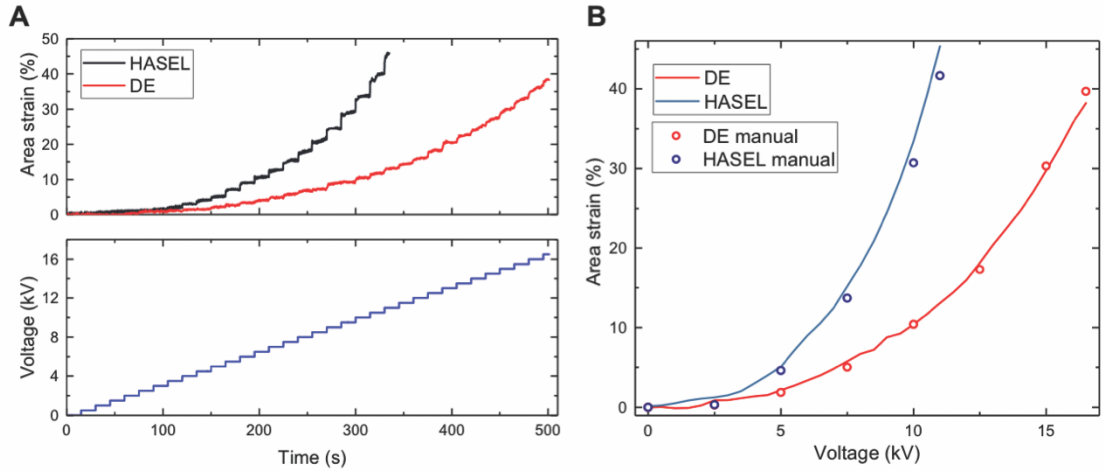


**Fig. S7. Comparison of circular DE and circular HASEL actuators.** (A) A stepped voltage signal was applied to circular DE and HASEL actuators. Each step was 0.5 kV with 15 s between steps (bottom). Actuation was recorded with a camera and the area strain (top) was measured using an image processing program written in MATLAB. (B) Accuracy of the area strain measured with the image processing program (solid lines) was verified by manually measuring area strain at several voltages (data points).

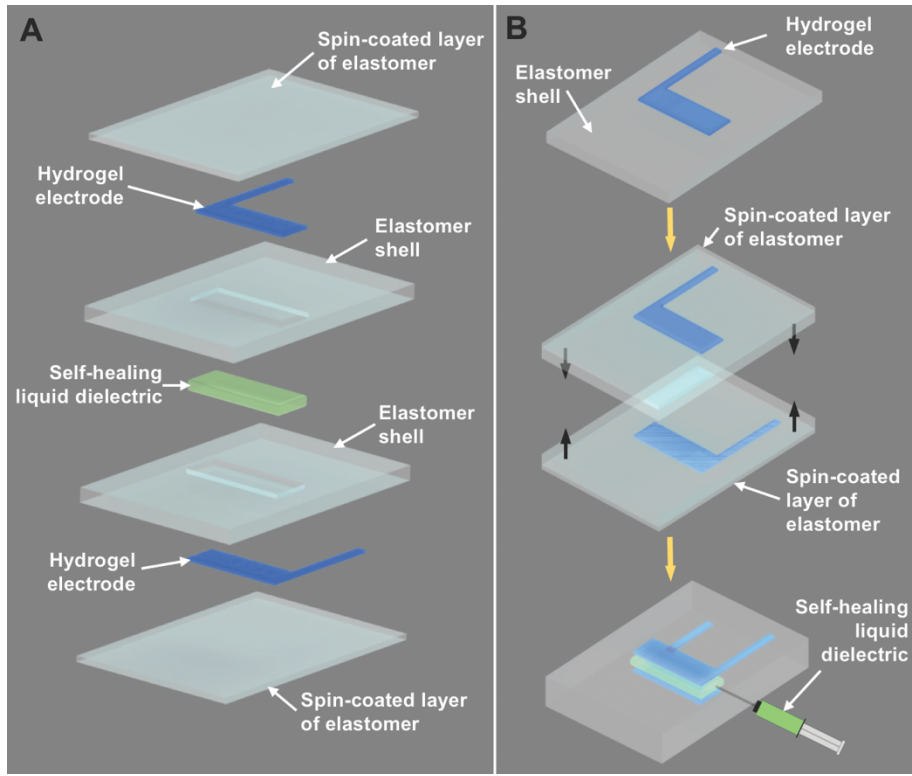


**Fig. S8. Components of a single-unit planar HASEL actuator.** (A) Exploded view of planar HASEL actuator with each component labeled. (B) Illustration of the major steps of HASEL actuator fabrication.

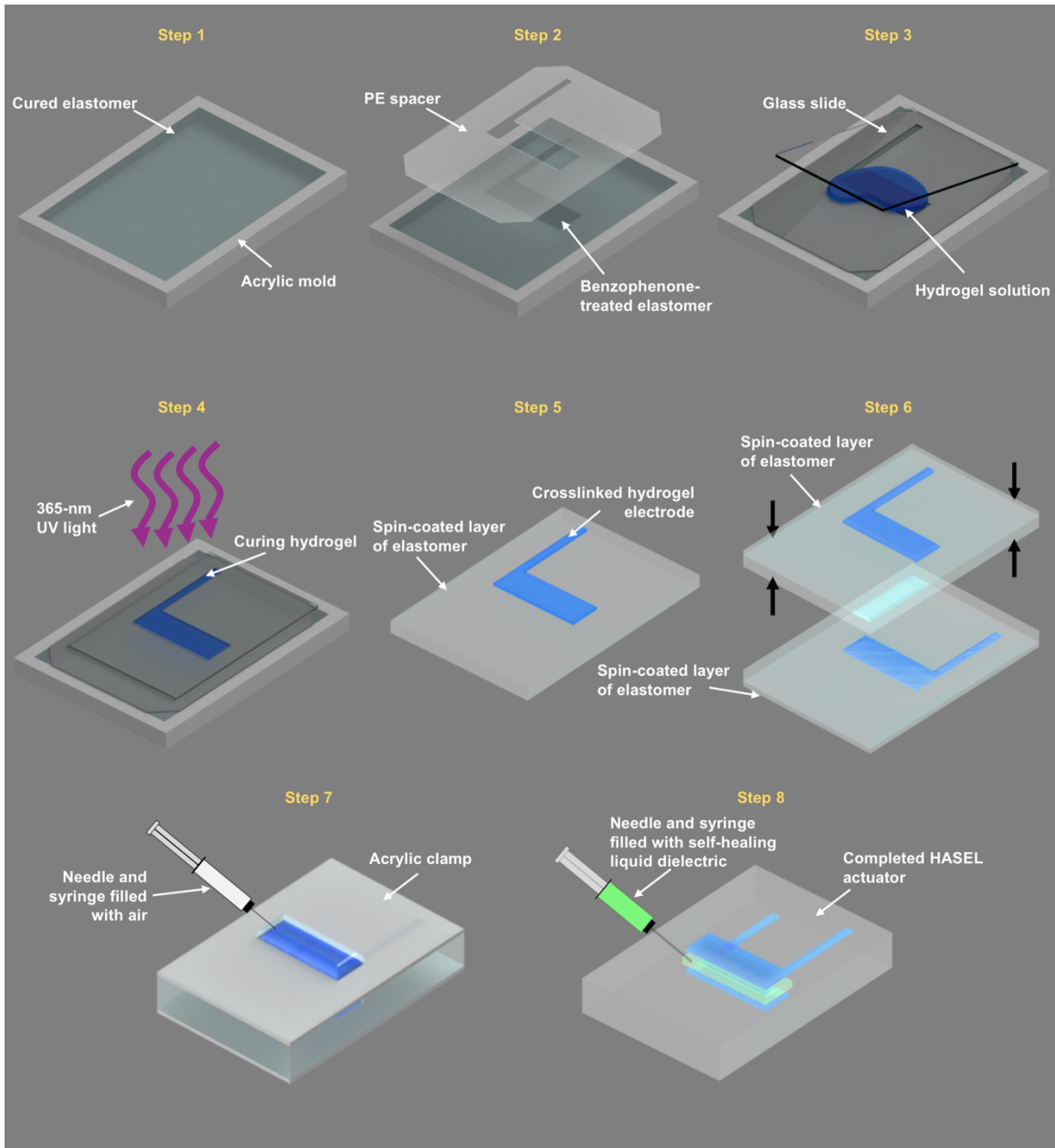


**Fig. S9. Fabrication steps for a single-unit planar HASEL actuator:** **Step 1** –Ecoflex 00-30 is cast into an acrylic mold (6 cm wide x 9 cm long x 0.8 mm deep), then cured in the oven for 10 minutes at 70 °C. **Step 2** – Treat the elastomer with a benzophenone solution (10 wt% in ethanol) as described in the *Stretchable electrodes* section. Then align a laser cut PE spacer with the treated area of the elastomer. **Step 3** – Apply the hydrogel solution and cover with a glass slide. Clamps can be used to hold the glass slide in place.

**Step 4** – Cure the hydrogel under 365-nm UV light for 1 hour. **Step 5** – Spin-coat a thin layer of Ecoflex over the cured hydrogel for encapsulation. **Step 6** – With the electrodes facing outwards, bond the elastomer sheets together using uncured Ecoflex 00-30. Hold the two pieces together using acrylic pieces. **Step 7** – A syringe with a needle is used to create an air-filled pouch between the electrodes. Cure the assembly in an oven for 10 min at 70 °C. **Step 8** – Remove the acrylic clamp and use a needle with a syringe to remove the air from the chamber and refill it with 1.2 mL of liquid dielectric.



**Fig. S10. Actuation of a six-unit planar HASEL actuator.** Quasi-static linear actuation of a six-unit planar HASEL actuator is shown at 11.5 kV with a 500 g load. Lateral prestretch was fixed at 2.5 and there was an initial prestretch of 1.5 in the direction of the weight. The use of six units made it easier to operate actuators in different orientations, because change in hydrostatic pressure of the liquid is small. Liquid dielectric may get pushed to one side resulting in regions of the HASEL actuator that bulge outward.

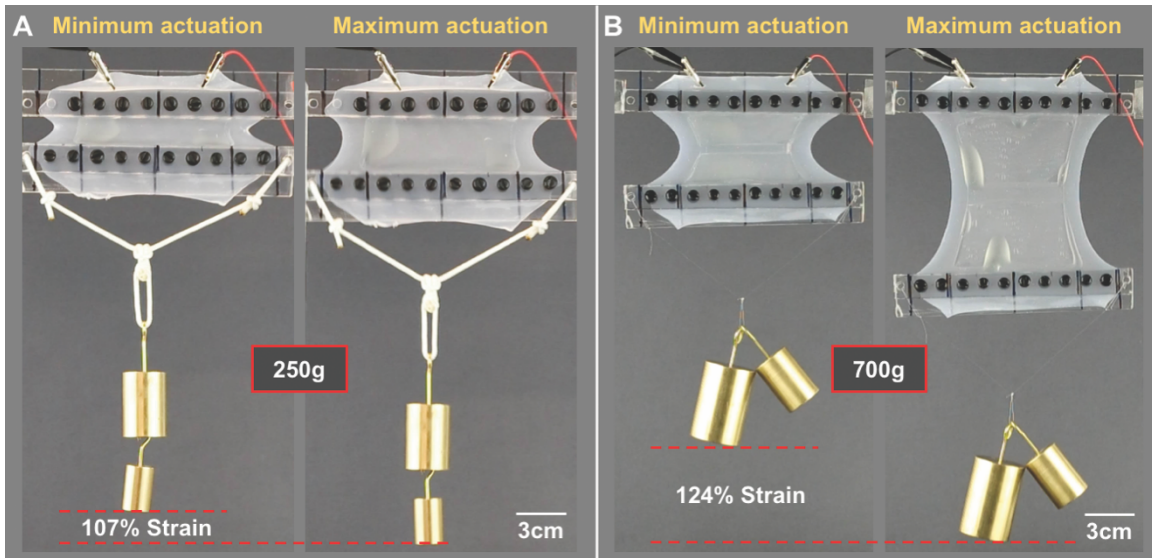


**Fig. S11. Dynamic actuation of single-unit and two-unit planar HASEL actuators.** **(A)**

A single-unit planar HASEL actuator was driven by a sinusoidal signal with frequency set near resonance and achieved 107% linear strain under a 250 g load (actuation stress  $\sim$ 32 kPa). Amplitude of the voltage was 13 kV, which corresponds to an applied field of 10.1 kV/mm (based on un-deformed thickness of the actuator). The actuation frequency was 4.6 Hz. **(B)** A two-unit planar HASEL actuator was driven by a sinusoidal signal with frequency set near resonance and achieved 124% linear strain with a 700 g load (actuation stress  $\sim$ 114 kPa). Amplitude of the voltage was 14.5 kV, which corresponds to an applied field of 15.5 kV/mm (based on un-deformed thickness of the actuator), and the frequency was 2.7 Hz.

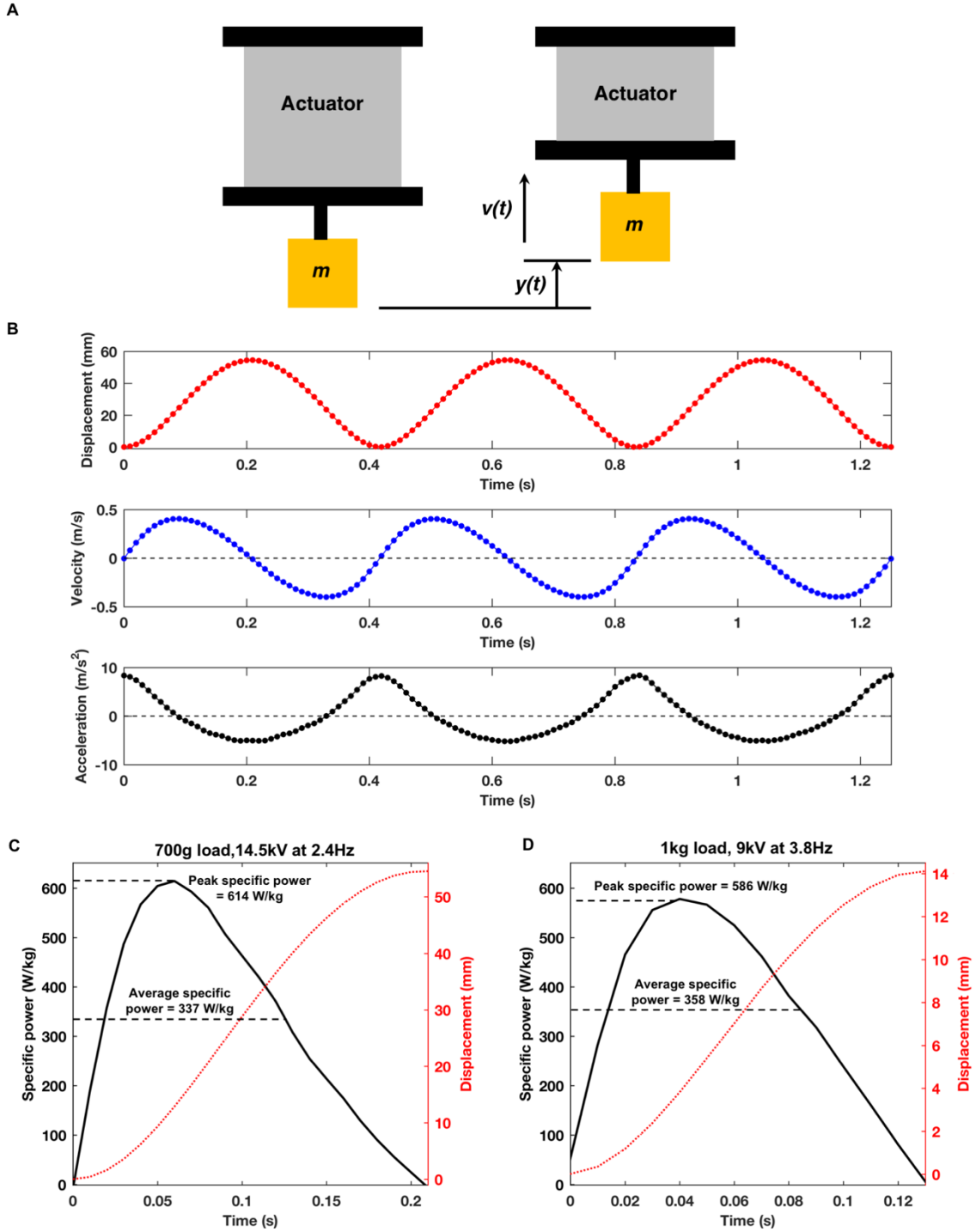


**Fig. S12. Measurement of specific power and work of HASEL actuators.** (A) Gravimetric power and work were measured for a planar HASEL actuator lifting a mass,  $m$ . The actuator was driven by a sinusoidal voltage signal. (B) Displacement was measured

using a high-speed camera (Model Phantom v710, Vision Research). Velocity and acceleration were calculated from the displacement data. The time histories for displacement, velocity, and acceleration are shown for a two-unit planar HASEL actuator lifting a 700 g load. **(C)** Plot of specific power during contraction for a two-unit planar HASEL actuator lifting 700 g. **(D)** Plot of specific power during contraction for a single-unit planar HASEL actuator lifting 1 kg.

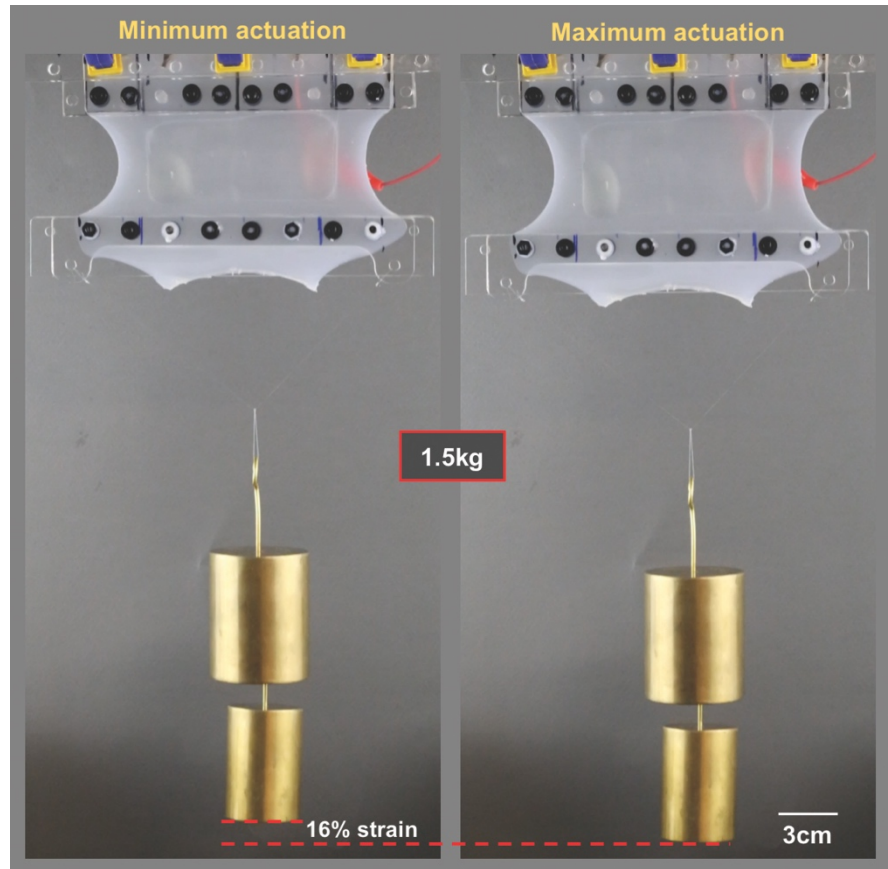


**Fig. S13. Actuation of a single-unit planar HASEL actuator under high load.** A single-unit planar HASEL actuator could lift a 1.5 kg load. The amplitude of the applied sinusoidal voltage signal was 9 kV which corresponds to a maximum applied field of  $\sim 26$  kV/mm (based on un-deformed thickness of the actuator) and the actuation frequency was 3.8 Hz. The actuation frequency was near the resonant frequency of the system. Actuation stress at equilibrium was 0.30 MPa and maximum linear strain was 16%. Lateral prestretch was fixed at 3 and there was an initial prestretch of 3.5 in the direction of the weight.

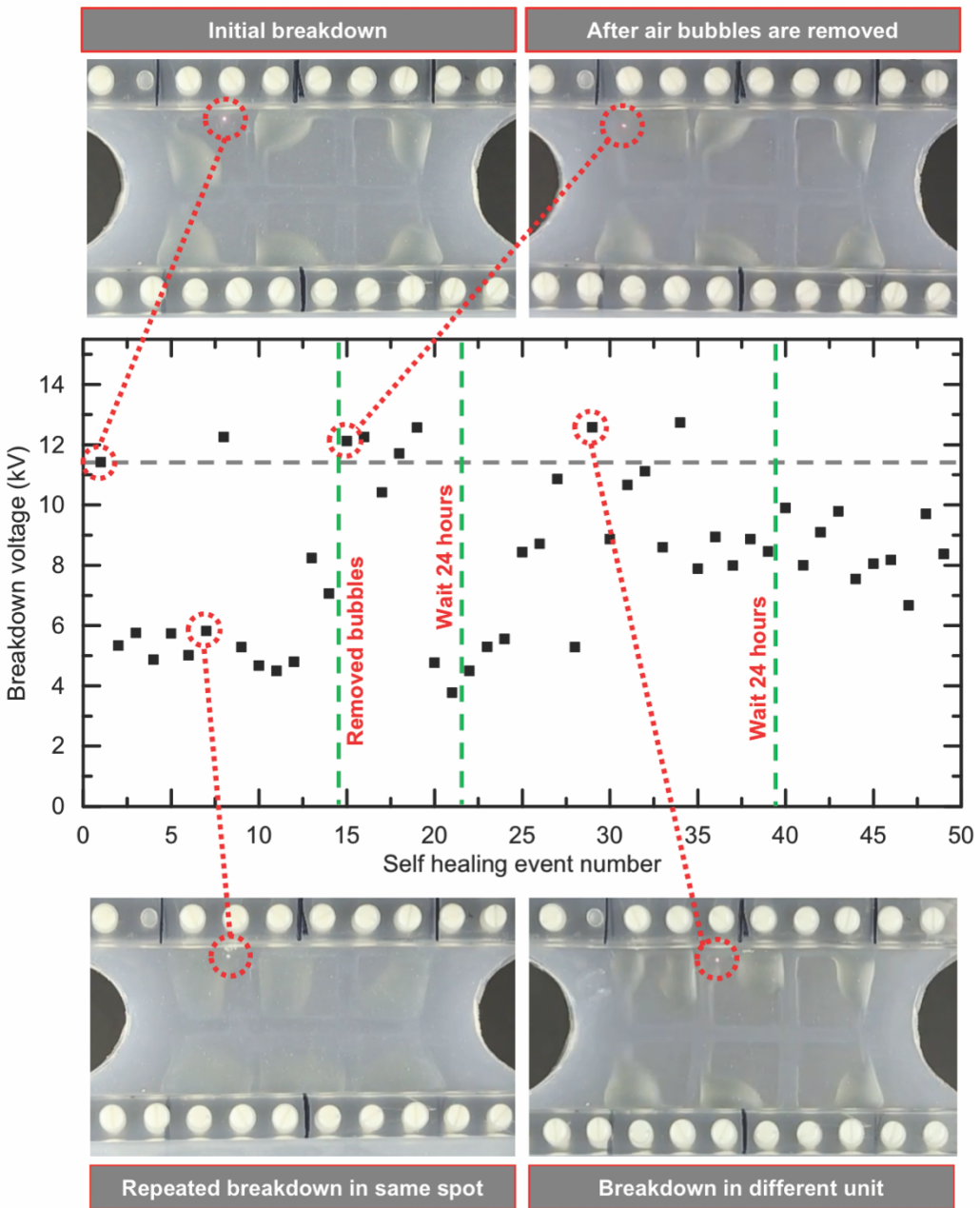


**Fig. S14. Self-healing of a six-unit planar HASEL actuator.** A linear voltage ramp at a rate of 0.5 kV/s was applied until dielectric breakdown occurred. After 1 minute, another linear voltage ramp was applied until dielectric breakdown. This was repeated for 50 cycles to evaluate the self-healing performance of the six-unit planar HASEL actuator. Gas bubbles formed after dielectric breakdown occurred (upper-left image). These bubbles

have a lower breakdown strength, and electrical breakdown occurred in the same location but at lower voltages (lower-left image). After the gas bubbles were removed, electrical breakdown occurred at a higher voltage and in a different location (top-right image). Electrical breakdown can also occur at a different location and at voltage higher than initial breakdown voltage and without removing any gas bubbles (lower-right image).

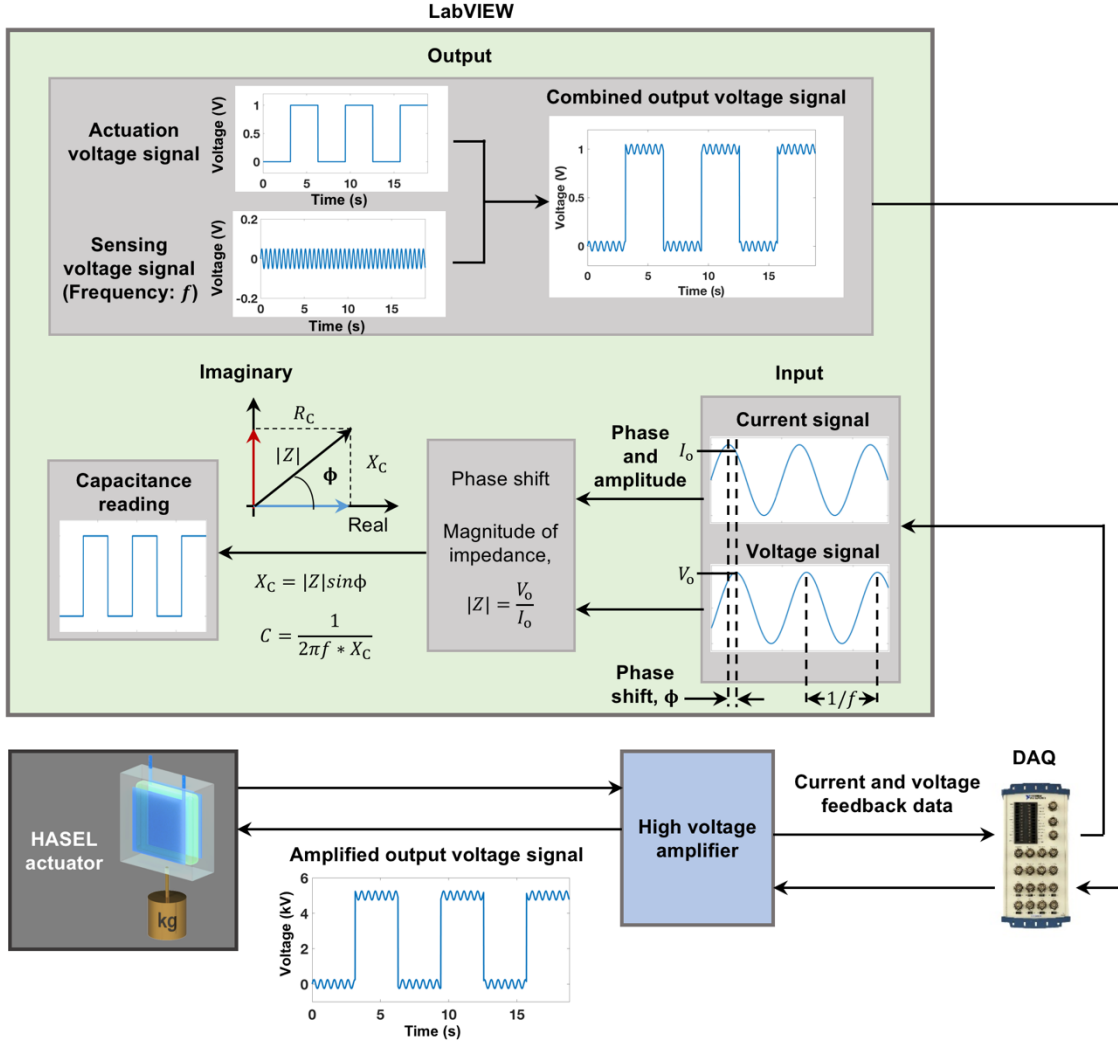


**Fig. S15. Schematic view of the software and hardware used for self-sensing of HASEL actuators.** The actuation voltage signal and sensing voltage signal were combined in LabVIEW and output from a DAQ (Model USB-6212, National Instruments) to the high voltage amplifier, which had a constant gain of 5 kV/V. The amplified voltage signal was applied to the HASEL actuator. Current and voltage were monitored from the high voltage amplifier and input to the DAQ. Phase shift,  $\phi$ , and magnitude of the impedance,  $Z$ , were measured in LabVIEW and used to calculate the capacitive impedance,  $X_C$ . Capacitance was calculated based on capacitive impedance and frequency,  $f$ .

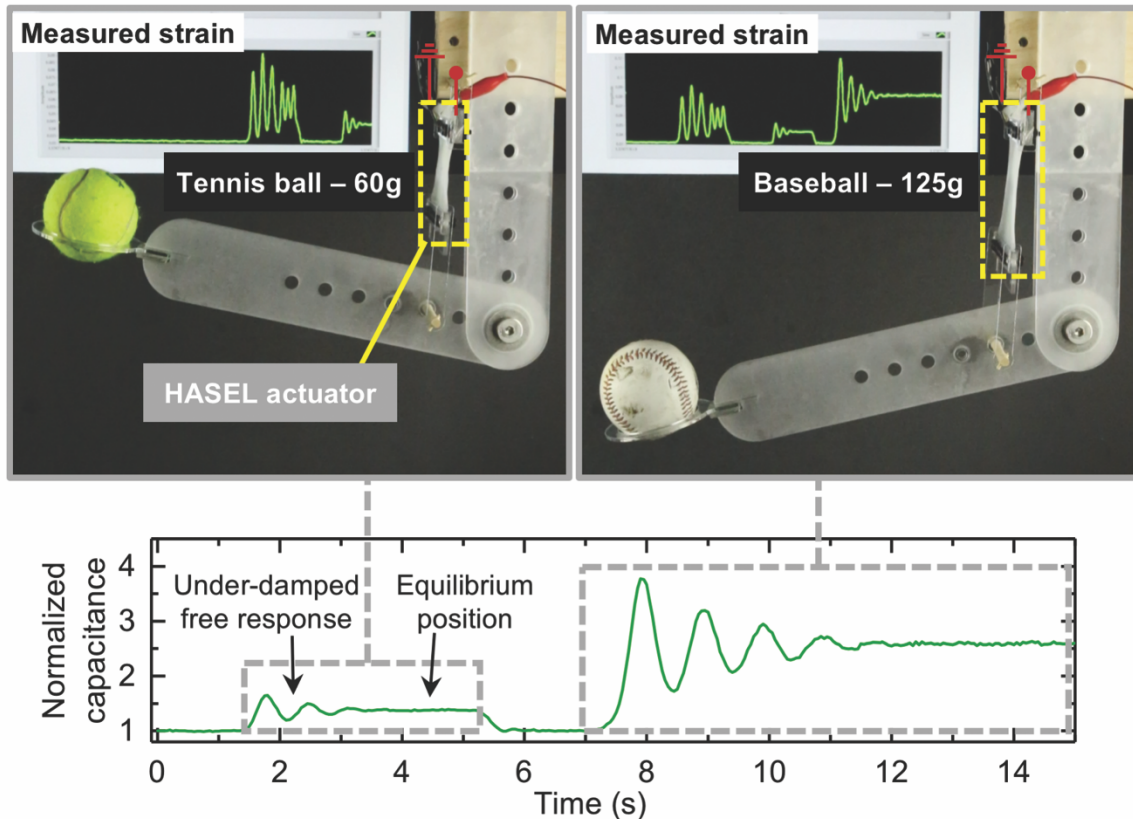


**Fig. S16. Sensing position of a robotic arm using a HASEL actuator.** A robotic arm powered by a planar HASEL actuator measured capacitance for different payloads. The actuation voltage signal was set to 0 kV while the sensing voltage signal was set to an amplitude of 0.08 kV and frequency of 2.5 kHz. Normalized capacitance measurements are plotted as a function of time, where normalized capacitance is the instantaneous capacitance value divided by the capacitance of the arm without any loading. A tennis ball (60 g) was dropped onto a holder at the end of the arm. The plot shows the under-damped free response of the arm which settles to an equilibrium capacitance value. The tennis ball was removed and a baseball (125 g) was placed onto the end of the arm. At equilibrium, the normalized capacitance measured from the baseball was more than double the value for the tennis ball.

### **Movie S1**

The experimental setup shown in Fig. S5 was used to demonstrate dielectric breakdown through a solid dielectric (PDMS) and through a liquid dielectric (Envirotemp FR3). One T-pin was connected to ground while the other was connected to the high voltage amplifier. Voltage was increased linearly at 0.5 kV/s until dielectric breakdown. Dielectric breakdown through the solid dielectric (PDMS) occurred at 34.3 kV which resulted in permanent damage to the material. Dielectric breakdown through the liquid dielectric (Envirotemp FR3) occurred at 14.7 kV which produced a gas bubble that quickly dissipated and the liquid dielectric returned to its initial insulating state.

### **Movie S2**

A single donut HASEL actuator made of Ecoflex 00-30 with an electrode diameter of 1.5 cm was actuated, until dielectric breakdown occurred, at which point the device self-healed and continued to operate. The actuator was activated with a 0.5 Hz reversing square wave with varying amplitudes. Sequences of three breakdown cycles are shown:

**Cycle 1** – 15 kV, 18 kV, breakdown, self-heal

**Cycle 2** - 15 kV, 17 kV, breakdown, self-heal

**Cycle 3** – 15 kV, 18 kV, 20 kV, 22 kV

### **Movie S3**

A stack of five donut HASEL actuators with an electrode diameter of 2.5 cm was actuated with a 15 kV reversing square wave at 0.5, 5, 10, 15, and 20 Hz.

### **Movie S4**

Two stacks of five donut HASEL actuators were used as a soft gripper which was capable of delicately grasping a fresh raspberry and a raw egg. Each donut HASEL actuator had an electrode diameter of 1.5 cm. Before picking up the raspberry, the HASEL actuators were driven with a 1 Hz, 18 kV reversing square wave to demonstrate the gripping actuation, while an 18 kV DC signal was applied to grip and then transport the raspberry. The HASEL actuators were driven with a 20 kV DC signal to lift the raw egg then voltage was turned off to drop the egg.

### **Movie S5**

HASEL actuators were driven near their resonant frequency which amplified actuation response. A single-unit planar HASEL actuator lifted 250 g. The applied voltage signal was a 4.6 Hz sine wave with three different voltage amplitudes – 7, 10, and 13 kV. A two-unit planar HASEL actuator lifted 700 g. The applied voltage signal was a 2.7 Hz sine wave with two different voltage amplitudes – 9.0 and 14.5 kV.

### **Movie S6**

Six two-unit planar HASEL actuators were arranged in parallel to deliver large actuation force. The HASEL actuators lifted a gallon of water (~ 4 kg) which had been dyed with blue food coloring (McCormick) for visibility. The front view shows actuation of the device with a 2.5 Hz sine wave at an amplitude of 11.5 kV and 12.5 kV. The side view shows the six actuators operating at 2.7 Hz with an amplitude of 9.0 kV. Two planar HASEL actuators were mounted on a single clamp so that only three clamps were used,

which when viewed from the side, appears as though only three HASEL actuators were used.

### **Movie S7**

Two self-sensing planar HASEL actuators powered a robotic arm. The ‘driving voltage’ (red plot) shows the combined actuation voltage signal and sensing voltage signal. The ‘sensing signal’ (green plot) is the capacitance measured from the HASEL actuators. The HASEL actuators were connected to ground on one side and to the high voltage amplifier on the other. With the actuation voltage turned off, the arm measured changes in capacitance from the external force of a handshake. A tennis ball (60 g) and baseball (125 g) were used to show a change in capacitance from different loads. The arm was then actuated while holding the baseball. The actuation voltage signal was 1 Hz sine wave. Voltage amplitude started at 12.5 kV, was decreased to 10 kV, then further decreased to 8 kV before being turned off.

### **Movie S8**

Two self-sensing planar HASEL actuators powered a robotic arm. The ‘driving voltage’ (red plot) shows the combined actuation voltage signal and sensing voltage signal. The ‘sensing signal’ (green plot) is the capacitance measured from the HASEL actuators. The HASEL actuators were connected to ground on one side and to the HV amplifier on the other. With the actuation voltage turned off, the arm was manually moved and held at different positions. The change in capacitance from these movements is shown in the green plot.

## References

1. S. Kim, C. Laschi, B. Trimmer, Soft robotics: A bioinspired evolution in robotics. *Trends Biotechnol.* **31**, 287–294 (2013). [doi:10.1016/j.tibtech.2013.03.002](https://doi.org/10.1016/j.tibtech.2013.03.002) [Medline](#)
2. D. Trivedi, C. D. Rahn, W. M. Kier, I. D. Walker, Soft robotics: Biological inspiration, state of the art, and future research. *Appl. Bionics Biomech.* **5**, 99–117 (2008).  
[doi:10.1155/2008/520417](https://doi.org/10.1155/2008/520417)
3. D. Rus, M. T. Tolley, Design, fabrication and control of soft robots. *Nature* **521**, 467–475 (2015). [doi:10.1038/nature14543](https://doi.org/10.1038/nature14543) [Medline](#)
4. B. Mazzolai, L. Margheri, M. Cianchetti, P. Dario, C. Laschi, Soft-robotic arm inspired by the octopus: II. From artificial requirements to innovative technological solutions. *Bioinspir. Biomim.* **7**, 025005 (2012). [doi:10.1088/1748-3182/7/2/025005](https://doi.org/10.1088/1748-3182/7/2/025005) [Medline](#)
5. S. Bauer, S. Bauer-Gogonea, I. Graz, M. Kaltenbrunner, C. Keplinger, R. Schwödiauer, 25th anniversary article: A soft future: from robots and sensor skin to energy harvesters. *Adv. Mater.* **26**, 149–161 (2014). [doi:10.1002/adma.201303349](https://doi.org/10.1002/adma.201303349) [Medline](#)
6. J.-Y. Sun, C. Keplinger, G. M. Whitesides, Z. Suo, Ionic skin. *Adv. Mater.* **26**, 7608–7614 (2014). [doi:10.1002/adma.201403441](https://doi.org/10.1002/adma.201403441) [Medline](#)
7. B. Trimmer, A practical approach to soft actuation. *Soft Robot.* **4**, 1–2 (2017).  
[doi:10.1089/soro.2017.29011.bat](https://doi.org/10.1089/soro.2017.29011.bat) [Medline](#)
8. F. Ilievski, A. D. Mazzeo, R. F. Shepherd, X. Chen, G. M. Whitesides, Soft robotics for chemists. *Angew. Chem. Int. Ed.* **50**, 1890–1895 (2011). [doi:10.1002/anie.201006464](https://doi.org/10.1002/anie.201006464) [Medline](#)
9. P. Polygerinos *et al.*, Soft robotics: Review of fluid-driven intrinsically soft devices; manufacturing, sensing, control, and applications in human-robot interaction. *Adv. Eng. Mater.* **19**, 1700016 (2017). [doi:10.1002/adem.201700016](https://doi.org/10.1002/adem.201700016)
10. R. F. Shepherd, F. Ilievski, W. Choi, S. A. Morin, A. A. Stokes, A. D. Mazzeo, X. Chen, M. Wang, G. M. Whitesides, Multigait soft robot. *Proc. Natl. Acad. Sci. U.S.A.* **108**, 20400–20403 (2011). [doi:10.1073/pnas.1116564108](https://doi.org/10.1073/pnas.1116564108) [Medline](#)
11. C. S. Haines, M. D. Lima, N. Li, G. M. Spinks, J. Foroughi, J. D. W. Madden, S. H. Kim, S. Fang, M. Jung de Andrade, F. Göktepe, Ö. Göktepe, S. M. Mirvakili, S. Naficy, X. Lepró, J. Oh, M. E. Kozlov, S. J. Kim, X. Xu, B. J. Swedlove, G. G. Wallace, R. H. Baughman, Artificial muscles from fishing line and sewing thread. *Science* **343**, 868–872 (2014). [doi:10.1126/science.1246906](https://doi.org/10.1126/science.1246906) [Medline](#)
12. R. Pelrine, R. Kornbluh, Q. Pei, J. Joseph, High-speed electrically actuated elastomers with strain greater than 100%. *Science* **287**, 836–839 (2000).  
[doi:10.1126/science.287.5454.836](https://doi.org/10.1126/science.287.5454.836) [Medline](#)

13. G. Kovacs, L. Düring, S. Michel, G. Terrasi, Stacked dielectric elastomer actuator for tensile force transmission. *Sens. Actuators Phys.* **155**, 299–307 (2009).  
[doi:10.1016/j.sna.2009.08.027](https://doi.org/10.1016/j.sna.2009.08.027)
14. C. Keplinger, M. Kaltenbrunner, N. Arnold, S. Bauer, Capacitive extensometry for transient strain analysis of dielectric elastomer actuators. *Appl. Phys. Lett.* **92**, 192903 (2008).  
[doi:10.1063/1.2929383](https://doi.org/10.1063/1.2929383)
15. P. Brochu, Q. Pei, Advances in dielectric elastomers for actuators and artificial muscles. *Macromol. Rapid Commun.* **31**, 10–36 (2010). [doi:10.1002/marc.200900425](https://doi.org/10.1002/marc.200900425) [Medline](#)
16. W. Yuan, L. B. Hu, Z. B. Yu, T. Lam, J. Biggs, S. M. Ha, D. J. Xi, B. Chen, M. K. Senesky, G. Grüner, Q. Pei, Fault-tolerant dielectric elastomer actuators using single-walled carbon nanotube electrodes. *Adv. Mater.* **20**, 621–625 (2008). [doi:10.1002/adma.200701018](https://doi.org/10.1002/adma.200701018)
17. S. J. Dünki, Y. S. Ko, F. A. Nüesch, D. M. Opris, Self-repairable, high permittivity dielectric elastomers with large actuation strains at low electric fields. *Adv. Funct. Mater.* **25**, 2467–2475 (2015). [doi:10.1002/adfm.201500077](https://doi.org/10.1002/adfm.201500077)
18. S. Hunt, T. G. McKay, I. A. Anderson, A self-healing dielectric elastomer actuator. *Appl. Phys. Lett.* **104**, 113701 (2014). [doi:10.1063/1.4869294](https://doi.org/10.1063/1.4869294)
19. E. Y. Wu, R. P. Vollertsen, On the weibull shape factor of intrinsic breakdown of dielectric films and its accurate experimental determination—part I: Theory, methodology, experimental techniques. *IEEE Trans. Electron Dev.* **49**, 2131–2140 (2002).  
[doi:10.1109/TED.2002.805612](https://doi.org/10.1109/TED.2002.805612)
20. Z. Suo, Theory of dielectric elastomers. *Acta Mech. Solida Sin.* **23**, 549–578 (2010).  
[doi:10.1016/S0894-9166\(11\)60004-9](https://doi.org/10.1016/S0894-9166(11)60004-9)
21. X. Zhao, Q. Wang, Harnessing large deformation and instabilities of soft dielectrics: Theory, experiment, and application. *Appl. Phys. Rev.* **1**, 021304 (2014). [doi:10.1063/1.4871696](https://doi.org/10.1063/1.4871696)
22. J. T. B. Overvelde, T. Kloek, J. J. A. D’haen, K. Bertoldi, Amplifying the response of soft actuators by harnessing snap-through instabilities. *Proc. Natl. Acad. Sci. U.S.A.* **112**, 10863–10868 (2015). [doi:10.1073/pnas.1504947112](https://doi.org/10.1073/pnas.1504947112) [Medline](#)
23. C. Keplinger, T. Li, R. Baumgartner, Z. Suo, S. Bauer, Harnessing snap-through instability in soft dielectrics to achieve giant voltage-triggered deformation. *Soft Matter* **8**, 285–288 (2012). [doi:10.1039/C1SM06736B](https://doi.org/10.1039/C1SM06736B)
24. See supplementary materials.
25. F. Carpi, P. Chiarelli, A. Mazzoldi, D. De Rossi, Electromechanical characterisation of dielectric elastomer planar actuators: Comparative evaluation of different electrode materials and different counterloads. *Sens. Actuators Phys.* **107**, 85–95 (2003).  
[doi:10.1016/S0924-4247\(03\)00257-7](https://doi.org/10.1016/S0924-4247(03)00257-7)

26. J. D. W. Madden, N. A. Vandesteeg, P. A. Anquetil, P. G. A. Madden, A. Takshi, R. Z. Pytel, S. R. Lafontaine, P. A. Wieringa, I. W. Hunter, Artificial muscle technology: Physical principles and naval prospects. *IEEE J. Oceanic Eng.* **29**, 706–728 (2004). [doi:10.1109/JOE.2004.833135](https://doi.org/10.1109/JOE.2004.833135)
27. J.-S. Plante, S. Dubowsky, On the performance mechanisms of dielectric elastomer actuators. *Sens. Actuators Phys.* **137**, 96–109 (2007). [doi:10.1016/j.sna.2007.01.017](https://doi.org/10.1016/j.sna.2007.01.017)
28. S. Song, D.-M. Drotlef, C. Majidi, M. Sitti, Controllable load sharing for soft adhesive interfaces on three-dimensional surfaces. *Proc. Natl. Acad. Sci. U.S.A.* **114**, E4344–E4353 (2017). [doi:10.1073/pnas.1620344114](https://doi.org/10.1073/pnas.1620344114) [Medline](#)
29. S. J. A. Koh, C. Keplinger, R. Kaltseis, C.-C. Foo, R. Baumgartner, S. Bauer, Z. Suo, High-performance electromechanical transduction using laterally-constrained dielectric elastomers part I: Actuation processes. *J. Mech. Phys. Solids* **105**, 81–94 (2017). [doi:10.1016/j.jmps.2017.04.015](https://doi.org/10.1016/j.jmps.2017.04.015)
30. K. Zimmermann, I. Zeidis, C. Behn, in *Mechanics of Terrestrial Locomotion* (Springer, 2009), pp. 125–159.
31. S. Rosset, B. M. O'Brien, T. Gisby, D. Xu, H. R. Shea, I. A. Anderson, Self-sensing dielectric elastomer actuators in closed-loop operation. *Smart Mater. Struct.* **22**, 104018 (2013). [doi:10.1088/0964-1726/22/10/104018](https://doi.org/10.1088/0964-1726/22/10/104018)
32. M. M. Sadeghi, H. S. Kim, R. L. B. Peterson, K. Najafi, Electrostatic micro-hydraulic systems. *J. Microelectromech. Syst.* **25**, 557–569 (2016). [doi:10.1109/JMEMS.2016.2552141](https://doi.org/10.1109/JMEMS.2016.2552141)
33. F. Carpi, G. Frediani, D. De Rossi, Hydrostatically coupled dielectric elastomer actuators. *IEEE/ASME Trans. Mechatron.* **15**, 308–315 (2010). [doi:10.1109/TMECH.2009.2021651](https://doi.org/10.1109/TMECH.2009.2021651)
34. Y. Bai, B. Chen, F. Xiang, J. Zhou, H. Wang, Z. Suo, Transparent hydrogel with enhanced water retention capacity by introducing highly hydratable salt. *Appl. Phys. Lett.* **105**, 151903 (2014). [doi:10.1063/1.4898189](https://doi.org/10.1063/1.4898189)
35. H. Yuk, T. Zhang, G. A. Parada, X. Liu, X. Zhao, *Nat. Commun.* **7**, ncomms12028 (2016).